Switching Frequency Reduction Using Model Predictive Direct Current Control for High-Power Voltage Source Inverters

Matthias Preindl, Erik Schaltz, *Member, IEEE*, and Paul Thøgersen, *Senior Member, IEEE*

***Abstract*—In this paper, a novel current control approach called *model predictive direct current control* (MPDCC) is presented. The controller takes into account the discrete states of the voltage source inverter (VSI), and the current errors are predicted for each sampling period. Voltage vectors are selected by a graph algorithm, whereby the most appropriate vector is chosen based on an optimization criterion. However, this depends on whether the state of the system is transient or steady. In the first case, the current error should be minimized as fast as possible in order to obtain fast dynamics. In the latter one, the VSI switching behavior is optimized since the switching losses account for a large amount of the total converter losses in high-power drive systems. MPDCC has been developed for a general neutral-point isolated resistive–inductive load with an internal voltage source. For demonstration, the presented control strategy has been implemented on a small-scale permanent-magnet synchronous machine drive system with a two-level VSI. This new approach has several advantages. The most important one is that the switching frequency is reduced up to 70% compared to linear control combined with pulsewidth modulation. Second, MPDCC obtains fast dynamic responses, which are already known from, e.g., direct torque control.**

***Index Terms*—Current control, drive systems, model predictive control (MPC), switching frequency optimization.**

I. Introduction

CONTROL strategies on drive systems and power converters have been the subject of ongoing research for several decades. Linear control combined with modulation schemes and nonlinear control based on hysteresis bounds [1] have become the most frequently used concepts in industrial applications. Most of these concepts go back to research on analog hardware, which limited complexity. On the other hand, modern digital hardware (DSPs and microcontrollers) has become a state of the art and has been widely accepted as industrial standard.

The continuously increasing computation power of digital hardware allows the implementation of new and generally more complex control techniques, e.g., fuzzy [2], adaptive [3], sliding mode [4], and predictive control [5]. Generally, predictive control uses a system model which is used to predict the future behavior and to select the control action on the basis of an optimality criterion.

Usually, model predictive control (MPC) identifies a control concept which predicts future values of system states in discrete-time steps. The number of subsequent prediction steps is called the *prediction horizon* N [6] and is usually limited to a few sampling periods due to the small timescales in power electronic devices. The cost function (also known as quality or decision function) [6] provides the criterion for choosing the appropriate control action. The prediction sequences are evaluated with the aid of the cost function, and the one minimizing the cost function is selected. Most scientists appreciate also the natural handling of system constraints [7], which can simply be a part of the cost function.

Calculating the cost function can be very time consuming depending on its complexity. If it is solved online, the approach is called linear MPC. Explicit MPC refers to a strategy which is optimized offline depending on the system states and which is implemented with a search tree [7], [8]. Moreover, if applied to power converters, MPC can either be combined with a modulation scheme (usually pulsewidth modulation (PWM) [9]) or can directly take into account the discrete nature of power electronic devices [10], [11].

MPC strategies can vary considerably according to the application in question [12]. Literature on low-power servo drives [8], [13] or rectifiers [14] is typically directed toward high dynamics with an aggressive current control strategy aiming at avoiding oscillations known from linear control concepts. In contrast, switching frequency and relative torque ripple have a high priority in the case of converters with higher power ratings [15], [16]. Lower dynamic might be accepted if it leads to a reduction of the average switching frequency.

In the presented work, the novel model predictive direct current (dc) control (MPDCC) concept for high-power converters is suggested as an alternative to low-frequency linear current control combined with a modulation scheme (normally, a proportional–integral (PI) controller combined with PWM). Main emphasis was put on the reduction of the average

Manuscript received December 18, 2009; revised March 15, 2010 and June 11, 2010; accepted July 20, 2010. Date of publication September 2, 2010; date of current version June 15, 2011.

M. Preindl is with the Power Electronic Systems Laboratory, Swiss Federal Institute of Technology (ETH) Zurich, 8092 Zurich, Switzerland, and also with the Department of Energy Technology, Aalborg University, 9220 Aalborg, Denmark (e-mail: matthias.preindl@gmail.com).

E. Schaltz is with the Department of Energy Technology, Aalborg University, 9220 Aalborg, Denmark (e-mail: esc@et.aau.dk).

P. Thøgersen is with KK-Electronic A/S, 9220 Aalborg, Denmark (e-mail: patho@kk-electronic.com).

Color versions of one or more of the figures in this paper are available online at http://ieeexplore.ieee.org.

Digital Object Identifier 10.1109/TIE.2010.2072894

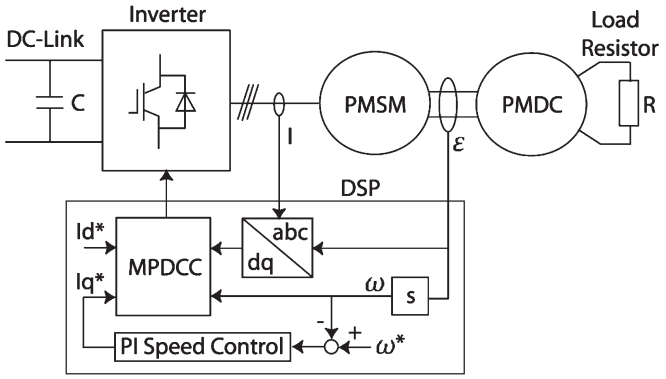

Fig. 1. Block diagram of the experimental demonstration system and control. The drive system contains a voltage source inverter, a PMSM, and a permanent-magnet dc load machine. The currents and rotor angle are measured for the machine control. The current control is made by the MPDCC, and for speed control, a linear PI controller is used.

switching frequency [17] as compared to the PI+PWM concept, whereby a similar current ripple for both models must be achieved.

In fan applications such as wind turbines, the torque is proportional to the squared angular speed $M \propto \omega^2$, and the power is proportional to the cubed speed $P = M\omega \propto \omega^3$, which means that the maximum power transfer and thus the maximum conduction losses are obtained at a maximum speed with the related high modulation indexes. On the other hand, grid-connected power converters work constantly with high modulation indexes. Heat sinks of an inverter are designed to cool the maximum power loss of the inverter, and with a constant switching frequency, it is found at the maximum speed. The switching losses depend on the current I_o in the insulated-gate bipolar transistor (IGBT) assuming a constant switching frequency f_s: $P_{Ls} = 1/2 U_d I_o f_s (t_{c(\mathrm{on})} + t_{c(\mathrm{off})})$ [18], where the voltage U_d is clamped by the dc voltage and the turn-on $t_{c(\mathrm{on})}$ and turnoff $t_{c(\mathrm{off})}$ times are device properties. The conduction losses $P_{Lc} = U_{\mathrm{on}} I_o t_{\mathrm{on}} / T_s$ [18] depend on the operation point (duty cycle), the current in the IGBT, and the conductive voltage drop U_{on} which is a device property. Thus, the maximum power loss with a permanent-magnet synchronous machine (PMSM) is obtained at a nominal machine speed, where the torque is high ($I_o \propto T \propto \omega^2$). Moreover, the switching losses themselves can be above 50% of the total converter losses [19], [20]. A control strategy with a switching reduction at high modulation indexes can thus significantly improve the efficiency of an inverter and increase the converter power density.

The MPDCC has been designed with a linear model for neutral-point isolated resistive–inductive loads with an internal voltage and takes into account the finite switching states of the converter. The block diagram of the experimental demonstration system is shown in Fig. 1. Moreover, some effort has been made to achieve an efficient problem formulation in order to solve the control problem online.

In this paper, the MPDCC principle is shown in Section II, and in Section III, the formulation and implementation are reported. In Section IV, an analytical function for calculating the minimum switching frequency is presented. In Section V, the results are shown.

II. Concept

Linear control combined with a PWM module causes some drawbacks. The constant switching frequency is interesting for filter issues but leads to unnecessary switching with the related losses. Moreover, large dead times in high-power converters cause a limited bandwidth of the current and speed controller.

In this section, a control strategy with focus on the optimization of the switching behavior is shown. Instead of using a PWM module, each inverter state change should be predicted in order to obtain a minimum number of changes. For this reason, a novel current controller has been developed. However, switching frequency optimization is only appropriated if the control goal is nearly achieved: in steady state where the gap between the current reference values and measured value is small. If the difference is big, i.e., in transients, the main control effort must be to minimize the control error. This distinction leads to a current error boundary, which defines if the system is in steady state or in transient state and can be illustrated as the boundary of direct torque control (DTC) at first sight.

MPDCC is used for prediction and takes into account the discrete states of the inverter. This approach is also named predictive direct control [21] or finite control set MPC [22] in literature. The MPC goal is to gain optimal control, but it can only be obtained with respect to a cost function. For this reason, the main challenge besides developing the control structure is to find a proper cost function in both cases, in transient and steady-state operations.

Last but not the least, the controller can be implemented in the $\alpha\beta$ or dq reference frame, leading to advantages and drawbacks, which will be presented in the following sections.

A. Error Prediction Based on a Graph Algorithm

For a given inverter state, i.e., the output voltage and the current error $\underline{e}[k] = \underline{i}^*[k] - \underline{i}[k]$, the current error of the next sampling period $\underline{e}[k+1]$ based on the load model can be predicted. Applying the calculation on each state vector, the one which generates the most convenience due to the cost function can be chosen.

However, the prediction of the eight possible errors is time demanding and not necessary. Suppose that, in an inverter state, it is not necessary to have the possibility to switch all possible inverter states in the next sampling period in order to control the current. It is enough to be able to switch the two neighbor vectors, which can also be obtained by changing only one leg state. However, if the actual state is a zero vector, all active vectors must be reachable in order to avoid spikes in the current ripple. The vectors which could be applied and for which further calculations are done depend on the actual inverter switching state, and the paths are given by the graph diagram in Fig. 2.

Moreover, voltage vectors are not set immediately but after executing the control algorithm or at the beginning of the next sampling period. Thus, the current error is modified during the algorithm execution by the voltage chosen in the last sampling period. This variation has to be taken into consideration in order

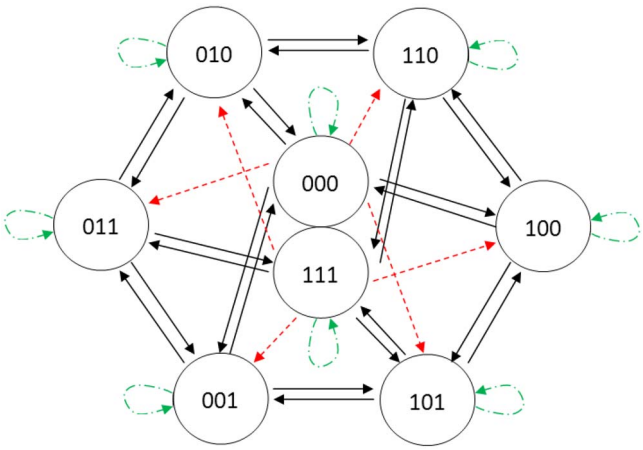

Fig. 2. Inverter state graph: Paths show the possible changes. (Double dashed line) No switching, (continuous line) one state change, and (dashed line) two state changes are necessary. The states, e.g., 100, refer to the switching state of each inverter leg, where 1 means that the upper transistor is *on* and the lower one is *off* and 0 indicates inverse switching states.

to improve the prediction accuracy and can be done with the load model and knowing the applied voltage vector.

B. Transient Operation

The converter is in transient operation if the current vector is outside a defined area (which will be defined later) around the current reference value, and the state is obtained by evaluating the current error vector.

If the converter is in transient state, the goal is to minimize as fast as possible the current error, and the voltage vector which leads to the smallest predicted error, i.e., reduces best the error, should be chosen. For this reason, a cost function is designed depending on the predicted current error, and the vector with the smallest cost will be applied.

C. Steady-State Operation

The converter is in steady-state operation if the current vector is within the appositely defined area. In steady-state operation, the current error is supposed to move in this area with the minimum possible switching, i.e., inverter state changes, and without leaving it.

The size of the area is given by the maximum admitted current ripple on both axes and can be a circle or a square. Also, a rectangle can be used if the current ripple is supposed to be different on both axes. Both the square and the circle lead to the same dq peak–peak current ripple if they have the same diameter, i.e., side length. Since the square has a bigger area compared to the circle, it is the preferred solution.

At steady state, the goal is to obtain the minimum possible state changes in order to maximally reduce the switching frequency. Thus, the converter should only change the state if the applied vector is going to drive the error out of the area in order to utilize the accepted current ripple.

If the state has to be changed, first, it is evaluated which vector given by the graph can be applied without leaving the area. Then, the vector should be chosen, which can be applied for the most time (usually, a few sampling periods) without leaving the steady-state area. The time how long a vector can be applied is obtained by extrapolating the machine, i.e., the load model, and formulated in a cost function, where the cheapest one of the possible vectors will be applied.

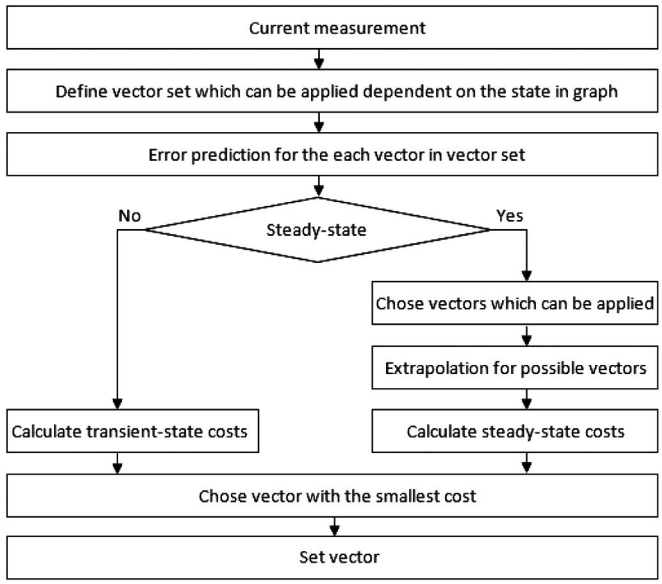

Fig. 3. MPDCC flowchart.

III. Design

In this section, the design and implementation of the MPDCC controller are shown, which can be done in the $\alpha\beta$ and dq reference frames, both with advantages and drawbacks. The main advantage is the constant inverter states in the $\alpha\beta$ reference frame, leading to faster computation since less transformations (one per inverter state) are required. On the other hand, the reference currents are usually given in the dq reference frame; a backside is the back conversion into $\alpha\beta$ values. Moreover, the handling of salient pole machines is more complex since the different inductances on the d- and q-axes depend on the electrical angle. The (reference-frame-independent) flowchart of the control algorithm is shown in Fig. 3.

A. Current Error Prediction

In this section, the equation set is shown, which is used for the current error prediction. It is shown in the dq reference frame. Prediction in the $\alpha\beta$ reference frame is obtained by converting the equations. The amplitude-invariant vector transformation is used in both cases. The internal voltage is laid on the q-axis, i.e., in the case of PMSM, the rotor flux is laid on the d-axis and provides the reference angle for the dq transformation.

The difference between the reference and actual current vectors is defined as an error on both axes. The current reference value $\underline{i}^*$ is assumed to be constant. $\underline{i}$ is the current vector, and $\underline{e}$ is the current error. The indexes d and q refer to the d- and q-axes, respectively

$$e_d[k] = i_d^* - i_d[k] \tag{1}$$
$$e_q[k] = i_q^* - i_q[k]. \tag{2}$$

The current and, thus, its error can be modified by applying a voltage vector. It can be used for minimizing the error or keeping it within a well-defined area. For this reason, the influence of each vector on the current can be predicted in order to choose the one with the expected effect. The basis for the prediction is the load model. Due to clearness, the equations are derived on the PMSM model and then generalized. R is the stator resistance, L is the inductance, $\underline{u}_{0,\ldots,7}$ is the inverter voltage depending on states 0–7, ψ is the flux generated by the permanent magnets, and ω is the electrical angular velocity

$$u_{d0,\ldots,7} = L_d \frac{di_d}{dt} + Ri_d - \omega L_q i_q \tag{3}$$

$$u_{q0,\ldots,7} = L_q \frac{di_q}{dt} + Ri_q + \omega L_d i_d + \omega\psi. \tag{4}$$

The current-driving voltage, i.e., the voltage on the inductances $\underline{u}_L$, depends on the applied inverter state, the resistive voltage drop, the cross coupling between the two axes, and the back electromotive force (EMF)

$$u_{Ld} = L_d \frac{di_d}{dt} = u_{d0,\ldots,7} - Ri_d + \omega L_q i_q \tag{5}$$

$$u_{Lq} = L_q \frac{di_q}{dt} = u_{q0,\ldots,7} - Ri_q - \omega L_d i_d - \omega\psi. \tag{6}$$

The constant inverter states in the $\alpha\beta$ coordinates must be transformed via a space vector, i.e., *Park* transformation, in order to get the dq values, where ϵ is the electrical angle

$$u_{d0,\ldots,7} = u_{\alpha 0,\ldots,7}\cos(\epsilon) - u_{\beta 0,\ldots,7}\sin(\epsilon) \tag{7}$$

$$u_{q0,\ldots,7} = u_{\alpha 0,\ldots,7}\sin(\epsilon) + u_{\beta 0,\ldots,7}\cos(\epsilon). \tag{8}$$

Over a defined time, the expected current change can be calculated by integration, which depends, above all, on the applied inverter state vector. The time which the voltage is applied is the sampling time period T_s. The changes in i_d and i_q are given by

$$\Delta i_d[k+1] = \left(u_{d0,\ldots,7}[k] - Ri_d[k] + \omega[k]L_q i_q[k]\right)\frac{T_s}{L_d} \tag{9}$$

$$\Delta i_q[k+1] = \left(u_{q0,\ldots,7}[k] - Ri_q[k] - \omega[k]L_d i_d[k] - \omega[k]\psi\right)\frac{T_s}{L_q}. \tag{10}$$

In the more general neutral-point isolated resistive–inductive loads with an internal voltage source, the following generalized prediction equations are defined, where the internal voltage source is $\underline{u}_i$. In this case, the load model can be applied to grid-connected power converters or active filters, where the internal voltage is the grid voltage or the terminal voltage, respectively

$$\Delta i_d[k+1] = \left(u_{d0,\ldots,7}[k] - Ri_d[k] + \omega[k]L_q i_q[k] - u_{id}\right)\frac{T_s}{L_d} \tag{11}$$

$$\Delta i_q[k+1] = \left(u_{q0,\ldots,7}[k] - Ri_q[k] - \omega[k]L_d i_d[k] - u_{iq}\right)\frac{T_s}{L_q}. \tag{12}$$

Thus, the current and its error can be predicted with the assumption of constant reference currents

$$e_d[k+1] = e_d[k] - \Delta i_d[k+1] \tag{13}$$

$$e_q[k+1] = e_q[k] - \Delta i_q[k+1]. \tag{14}$$

B. Runtime Compensation

A voltage vector is not set immediately after the current measurement but after the execution of the algorithm. Thus, the current error which is found when the chosen vector is applied is modified by the voltage chosen in the last sampling period. This variation should be taken into consideration in order to improve the error prediction accuracy.

The compensation is done knowing the current-driving voltage $\underline{u}_L$ and the algorithm execution time T_e. $\underline{e}_C[k]$ is the compensated error

$$e_{Cd}[k] = e_d[k] - u_{Ld}[k]\frac{T_e}{L} \tag{15}$$

$$e_{Cq}[k] = e_q[k] - u_{Lq}[k]\frac{T_e}{L}. \tag{16}$$

C. Cost Function

The cost function is the criterion of which the vector, i.e., the output voltage, will be applied to the load. For each vector, the cost is calculated, and the cheapest one will be chosen. Since, in the two converter states, two different objectives should be fulfilled, two cost functions are designed.

If a vector should not be applied due to the graph or because the error would leave the area in steady state, the cost of the vector is set to a high value, and thus, it will not be chosen.

1) Transient State: If the converter is in transient state, the goal is to minimize the current error as fast as possible. For this reason, the voltage vector which application leads to the smallest predicted error in the next sampling period is chosen

$$c_{0,\ldots,7} = |e_d[k+1]| + |e_q[k+1]|. \tag{17}$$

2) Steady State: In steady state, a vector should be chosen, which can be applied for the most time without leaving the defined steady-state area in order to obtain less possible inverter leg state changes. For this reason, it is evaluated first which vectors can be applied without leaving the area; the one which cannot get a high cost.

For vectors which can be applied at least one sampling period, the time how long they can be applied afterward is obtained by extrapolating the machine, i.e., the load model. The model for the extrapolation in the dq coordinates is shown in the following, where $t_{0,\ldots,7}$ is the expected time how long a vector can be applied. The equations for the extrapolation in the $\alpha\beta$ coordinates are the same, changing the indexes

$$e_d(t_{0,\ldots,7}) = e_d[k+1] - u_{Ld}[k]\frac{t_{0,\ldots,7}}{L_d} \tag{18}$$

$$e_q(t_{0,\ldots,7}) = e_q[k+1] - u_{Lq}[k]\frac{t_{0,\ldots,7}}{L_q}. \tag{19}$$

The extrapolation depends on the shape of the steady-state area, which can be a circle ($\alpha\beta$ implementation) or a square (dq implementation). The extrapolation for the first one is done by solving (20), where e_L is the diameter of the circle

$$e_L = \sqrt{e_d^2(t_{0,\dots,7}) + e_q^2(t_{0,\dots,7})}. \tag{20}$$

The result is given by

$$t_{0,\dots,7} = \frac{-b \pm \sqrt{b^2 - 4ac}}{2a} \tag{21}$$

where

$$a = \frac{u_{Ld}^2[k+1]}{L_d} + \frac{u_{Lq}^2[k+1]}{L_q} \tag{22}$$

$$b = -2\left(\frac{u_{Ld}[k+1]}{L_d} e_d[k+1] + \frac{u_{Lq}[k+1]}{L_q} e_q[k+1]\right) \tag{23}$$

$$c = e_q^2[k+1] + e_d^2[k+1] - e_L^2[k+1]. \tag{24}$$

The extrapolation for the latter criterion is done by solving (25) and (26), where e_L is the side length of the square

$$e_L = \left|e_d\left(t'_{0,\dots,7}\right)\right| \tag{25}$$

$$e_L = \left|e_q\left(t''_{0,\dots,7}\right)\right| \tag{26}$$

$$t'_{0,\dots,7} = \frac{L_d}{u_{Ld}[k+1]}\left(e_d[k+1] \pm e_L\right) \tag{27}$$

$$t''_{0,\dots,7} = \frac{L_q}{u_{Lq}[k+1]}\left(e_q[k+1] \pm e_L\right) \tag{28}$$

$$t_{0,\dots,7} = \min\left\{t'_{0,\dots,7}; t''_{0,\dots,7}\right\}. \tag{29}$$

(21), (27), and (28) have both positive and negative results where the positive one refers to the extrapolated time and should be taken for further calculations.

For this reason, it is evaluated first which vectors can be applied without leaving the area. From these vectors, the one which can be applied the most time is chosen. The used cost function is

$$c_{0,\dots,7} = \frac{1}{t_{0,\dots,7}}. \tag{30}$$

D. Improvement With a Peripheral

In this section, the possibility of improving the steady-state switching frequency with an apposite peripheral is shown. The switching frequency is minimum if the error moves within the limits of the steady-state area but get as close as possible to the borders using all of the permitted ripple. With the already presented algorithms and reasonable sampling frequencies of 30–50 kHz, this is not the case since switching is necessary if the applied vector cannot be applied for an entire sampling period. For this reason, a peripheral has been introduced which permits changing the inverter state at each, instead of discrete, switching instant.

The already presented MPDCC strategy can be extended with a peripheral which can apply two different vectors in one sampling period. The first vector is always the already applied one, where no switching is necessary. The following vector will then be calculated with the already shown methods. With an additional information, a duty cycle is defined how long the first vector should be applied, and it is obtained by extrapolation. This peripheral can be implemented in a field-programmable gate array of a DSP board.

IV. Ideal Minimum Switching Frequency

The absolute minimum switching frequency can be estimated with a best case consideration: The internal voltage $u_i = mU_{\mathrm{dc}}/2$ is aligned with an active voltage vector in a circular steady-state area. In this case, the active and passive vectors are described by the following equations, where m is the modulation index:

$$\|\underline{u}_{\mathrm{active}}\| = \frac{2}{3}U_{\mathrm{dc}} - \frac{m}{2}U_{\mathrm{dc}} \tag{31}$$

$$\|\underline{u}_{\mathrm{passive}}\| = -\frac{m}{2}U_{\mathrm{dc}}. \tag{32}$$

Assuming to have a current error on the border of the circle, i.e., its absolute value is equal to the radius and the internal voltage pointing orthogonally outward, the best sequence which can be applied is first to choose the active vector (31) and then the passive one (32). Assuming to be able to use the whole diameter of the circle, it can be calculated how long each vector can be applied and, above all, how long the vector sequence can be applied, exploiting optimally the back EMF.

The equations which describe how long the given vectors need to cross over the circle (diameter Δi_{pp}) can be derived from (31) and (32). Initially, the active vector will be applied, and it is applied for time t; afterward, the passive vector is applied, which is applied for time $T - t$, where T is the total application time for the sequence

$$\Delta i_{pp} = \|\underline{u}_{\mathrm{active}}\|\frac{t}{L} = \left(\frac{2}{3}U_{\mathrm{dc}} - \frac{m}{2}U_{\mathrm{dc}}\right)\frac{t}{L} \tag{33}$$

$$\Delta i_{pp} = \|\underline{u}_{\mathrm{passive}}\|\frac{T-t}{L} = \left(-\frac{m}{2}U_{\mathrm{dc}}\right)\frac{T-t}{L}. \tag{34}$$

Since time t must be equal for both equations, the application time for both vectors T can be calculated

$$T = \Delta i_{pp} L\left(\frac{1}{\frac{2}{3}U_{\mathrm{dc}} - \frac{m}{2}U_{\mathrm{dc}}} + \frac{1}{-\frac{m}{2}U_{\mathrm{dc}}}\right). \tag{35}$$

The switching frequency can be calculated from the number of inverter state changes n that are necessary to obtain the sequence. For applying a sequence of two vectors, a minimum of two state changes $n = 2$ are necessary. Knowing these parameters, the absolute minimum switching frequency can be calculated

$$f_{\mathrm{switch}} = \frac{n}{6T}. \tag{36}$$

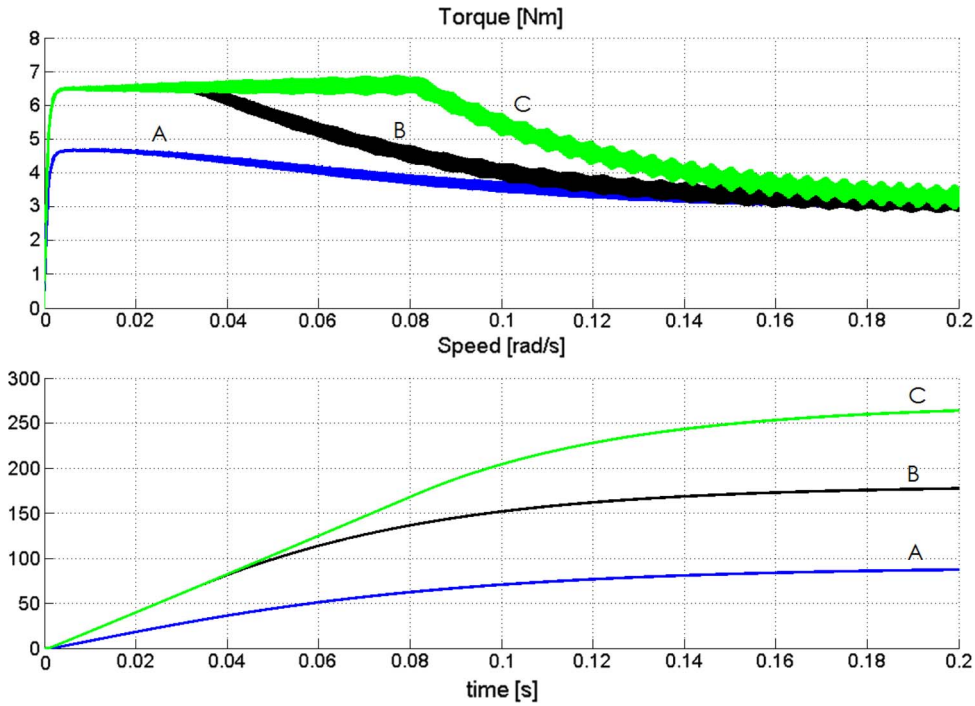

Fig. 4. Simulation result: Torque and electrical speed with the cascade PI control and PWM module applying three speed reference steps with modulation index 0 to (A) 0.29, (B) 0.57, and (C) 0.86, i.e., the electrical speeds 0 rad/s to 90, 180, and 270 rad/s.

The obtained switching frequency f_{switch} can be seen as an absolute minimum frequency, which is obtained with heavy ideal assumptions (the back EMF is parallel with one vector, the vectors reach the border of the optimization area, and that for obtaining the next vector, only one inverter leg change is always necessary), which are not feasible with discrete sampling times and discrete state inverters. For this reason, the obtained frequency gives the absolute minimum switching frequency.

V. Results

The designed control strategy has been tested and compared to PI+PWM control experimentally on a three-pole-pair PMSM. The nominal parameters of the experimental platform are 310-V inverter dc voltage, 3.7-A nominal current, 30- and 38-mH d and q inductances, respectively, and the 0.495-Wb flux generated by the permanent magnets.

A. Benchmark Reference: Cascade PI Control With PWM

A cascade PI controller has been applied and tested on the simulation and experimental platform: the PMSM drive system, in order to confirm the proper work. The current control is done with two PI controllers and feed-forward paths to decouple the d- and q-axes for independent control action. The speed control loop is done with a PI controller, and the PI controllers of both loops are tuned by plotting the Bode plot of the open-loop transfer function. The P-gain has been chosen in order to obtain a crossover frequency with a safety margin to dead times, and the I-gain has been chosen in order to get critical damping behavior, i.e., the highest gain without overshoots and ringing. Since cascade PI control is a widely employed and accepted control strategy, it has been used as a benchmark reference for further tests.

PI control with 10% worst case dq peak–peak current ripple, i.e., 0.37 A, is obtained with a switching frequency of 3.3 kHz (sampling frequency of 6.6 kHz) on the given system. However, the PMSM is a small salient pole machine, where the current ripple is different on the d- and q-axes; the average value has been taken for evaluation. To test control and the system, positive speed reference steps have been applied to the machine, and they are shown in Figs. 4 and 5.

B. MPDCC Evaluation

In this section, the MPDCC results are shown, which are obtained with the dq implementation and a squared steady-state area with a side length of 10% of the nominal current. For speed control, a PI controller has been designed with similar parameters as for the cascade PI one for better comparison even if the speed loop of MPDCC could be designed much faster. The sampling frequencies are 50 kHz in the simulation and 30 kHz in the experimental system due to computational constraints. A high sampling frequency is advantageous at steady state since the current variation over one sampling period is smaller, and the accepted current ripple can be used better. In order to evaluate MPDCC, speed reference steps are applied, which are shown in Figs. 6 and 7.

C. Switching Frequency Evaluation

The switching frequency was evaluated at steady state since it causes large losses. The power loss due to inverter switching state changes and the average switching frequency per IGBT are proportional; a control algorithm should use the smallest

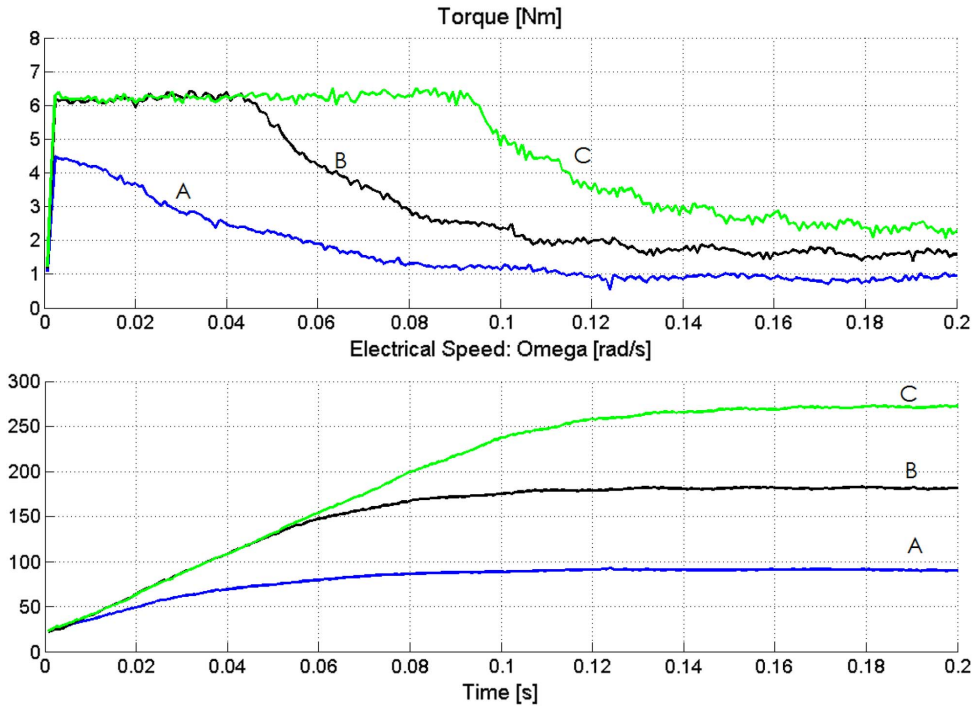

Fig. 5. Experimental result: Torque and electrical speed with the cascade PI control and PWM module applying three speed reference steps with modulation index 0.1 to (A) 0.29, (B) 0.57, and (C) 0.86, i.e., the electrical speeds 10 rad/s to 90, 180, and 270 rad/s. The reference steps do not start from zero due to an initialization procedure of the incremental encoder. The torque is calculated from the current measurements, where synchronous sampling [23] is used for filtering, and thus, the real current ripple cannot be evaluated in this graph. Moreover, the measurements are undersampled, i.e., not each sampling is stored due to the limited memory of the used DSP board.

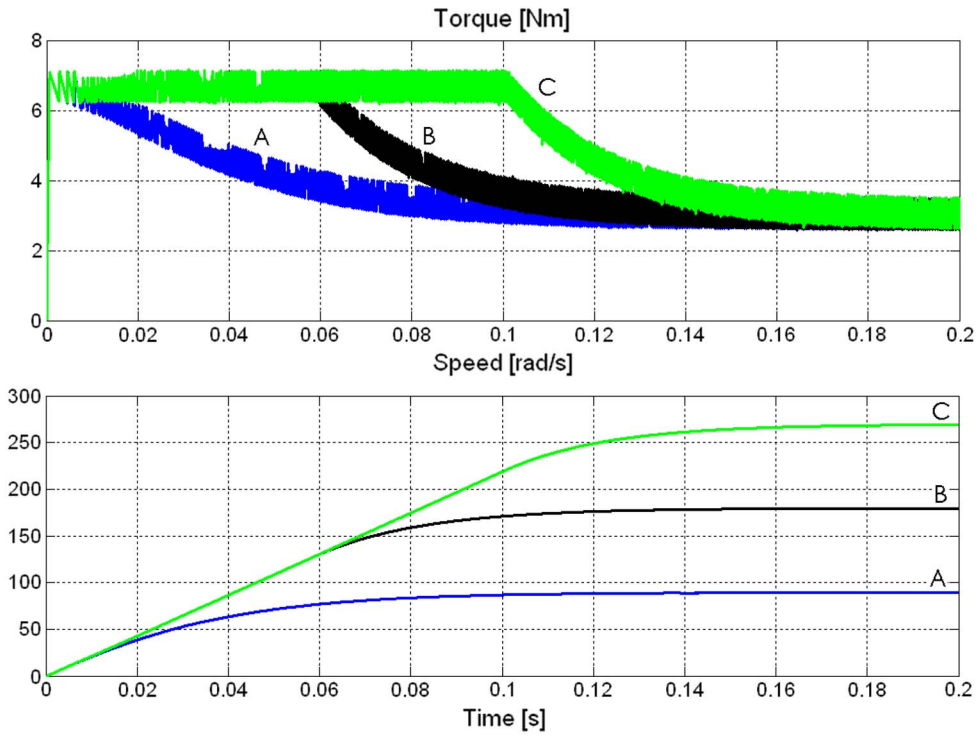

Fig. 6. Simulation result: Torque and electrical speed with the MPDCC applying three speed reference steps with modulation index 0 to (A) 0.29, (B) 0.57, and (C) 0.86, i.e., the electrical speeds 0 rad/s to 90, 180, and 270 rad/s.

possible number of state changes in order to achieve a predefined peak–peak current or torque ripple (10%).

For this reason, the total number of transistor state changes is summed up in a 0.05-s steady-state period. From these values, the average switching frequency for each transistor can be calculated. The results for PI+PWM, different implementations of MPDCC, and the best case switching limit are shown in Fig. 8.

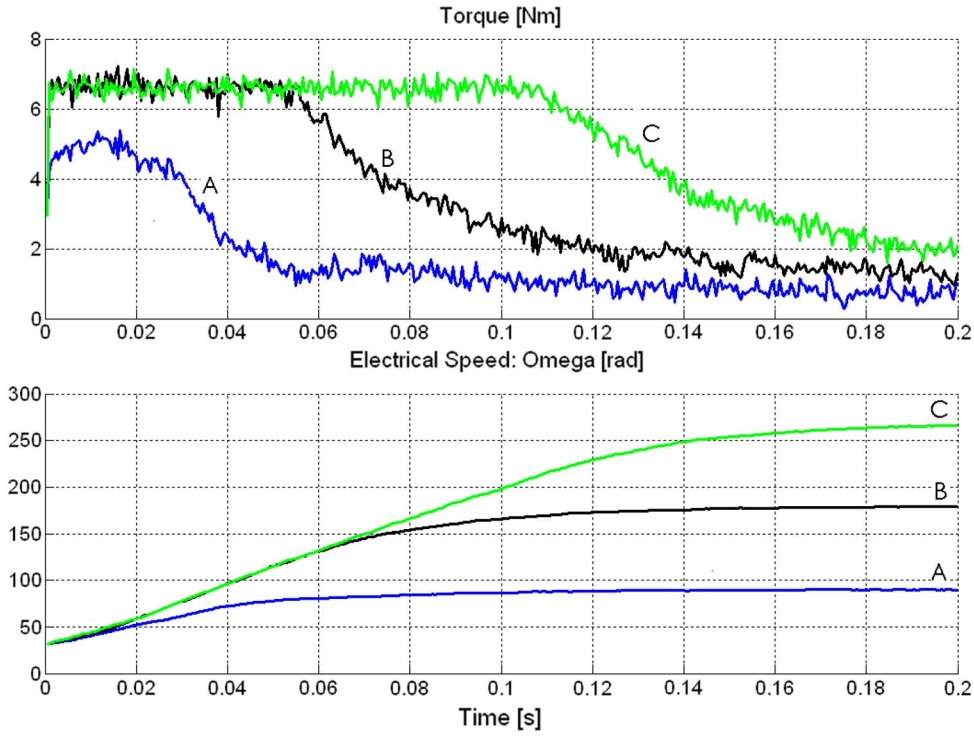

Fig. 7. Experimental result: Torque and electrical speed with the cascade PI control and PWM module applying three speed reference steps with modulation index 0.1 to (A) 0.29, (B) 0.57, and (C) 0.86, i.e., the electrical speeds 10 rad/s to 90, 180, and 270 rad/s. The reference steps do not start from zero due to an initialization procedure of the incremental encoder. Moreover, the measurements are undersampled, i.e., not each sampling is stored due to the limited memory of the used DSP board.

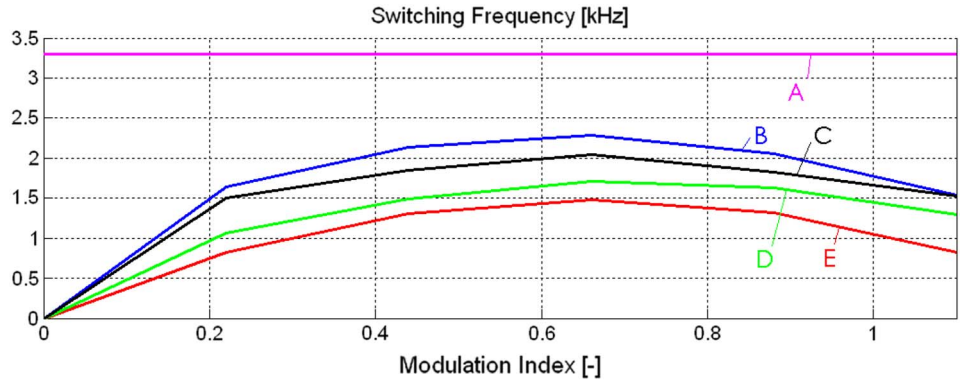

Fig. 8. Steady-state switching frequency. (A) Cascade PI control with the PWM module (experimental result). (B) MPDCC (experimental result). (C) MPDCC (simulation result). (D) MPDCC with an external module for applying two vectors in one sampling period (simulation result). (E) Ideal minimum switching frequency (F). All MPDCC results have been obtained with the implementation in the dq reference frame and 30-kHz sampling frequency.

Comparing the simulation and experimental results, the switching frequency is higher in the latter ones. This is mainly caused by the runtime compensation, which is more formidable on the experimental setup since the current measurement, i.e., the analog–digital conversion, is not done instantaneously but takes a few microseconds. The capacitive currents during switching are another challenge; thus, the current measurement must be avoided close to the switching interval.

D. Harmonic Analysis

In this section, a Fourier analysis is done in order to evaluate and compare the spectrum, which is generated by MPDCC and by the cascade PI controller with the PWM module. The experimental results are obtained with modulation index $m = 0.86$ (270-rad/s electrical speed) and the 0.3-p.u. (1.1-A) steady-state current. Noise is observed in most bandwidths but on different levels in both approaches with peaks at the 5th, 7th, 11th, 13th, etc., harmonics.

The waveform and spectrum of the MPDCC (dq implementation) currents are shown in Fig. 9. The spectrum is similar to the one of DTC. The total harmonic distortion (THD) is 9.8%. The spectrum and the waveform shown in Fig. 10 are obtained with the cascade PI control with the PWM module. The spectrum is typical for currents created by a PWM module. The noise is even low, but large harmonics are found around the switching frequency and its integer multiples. The THD is 8.0%.

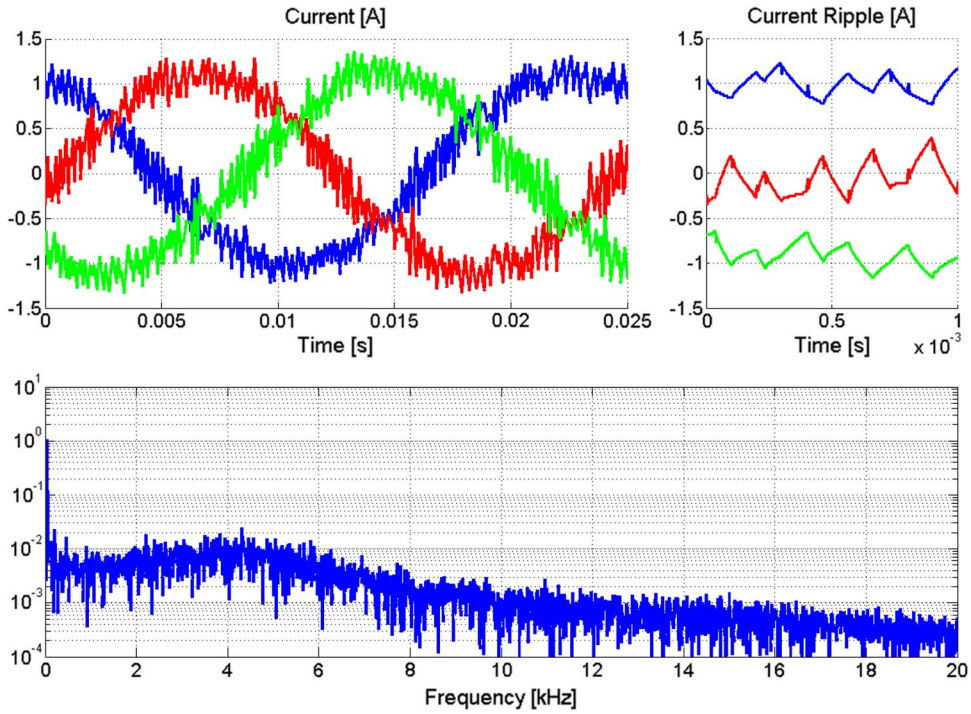

Fig. 9. Experimental result: Fourier analysis of the MPDCC currents.

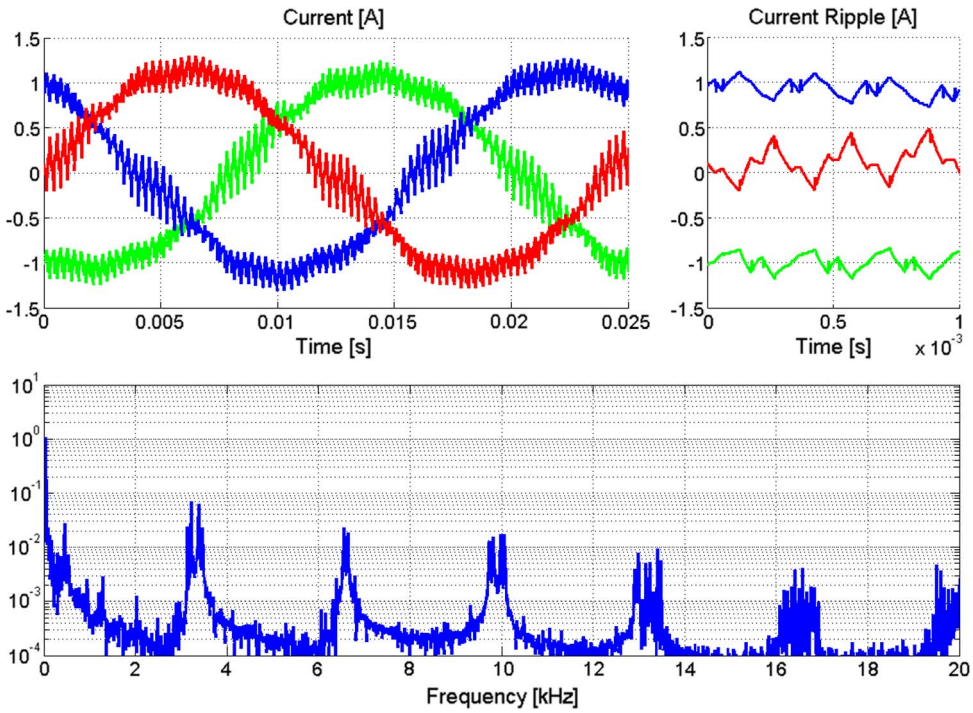

Fig. 10. Experimental result: Fourier analysis cascade PI control with PWM currents.

The PWM leads to a well-defined harmonic spectrum with peaks at the switching frequency. The harmonic spectrum of MPDCC shows higher noise due to the statistical control approach but no peaks. Even if it cannot be decided which spectrum is worse or better, the filter design for MPDCC is more competitive since peaks are missing. Moreover, the THD of MPDCC is lightly worse than the one of PI+PWM.

VI. Conclusion

In this paper, MPDCC which takes into account the discrete states of the inverter has been developed. Possible inverter states for application are identified by a graph algorithm, and their effects are predicted with the load model. Depending on whether the system states are transient or steady, an optimized cost function is used to evaluate and choose the appropriate vector.

The main advantage of MPDCC is the reduction of the average switching frequency up to 70% depending on the modulation index. This effect is particularly significant where the modulation indexes are low and high. This is particularly interesting for high-power converters, where the power loss due to switching is high. In particular, in fan applications, efficiency and converter power density can be significantly increased. Second, MPDCC leads also to a fast dynamic which can be compared to the fast responses of DTC, but it has not been focused since fast speed control is not a main issue in wind turbine applications.

However, the presented algorithm comes also with some drawbacks. One disadvantage is the required sampling period of 30–50 kHz and which increases as the ripple should be smaller. Moreover, the computation is more complex than the one of a linear controller. Control hardware with the appropriate computation capacities is required, and it is found in widely used DSP boards.

MPDCC can be improved using a two-step-ahead prediction in order to further reduce the switching frequency and to simplify the graph algorithm for the passive states. In a future work, this technique can also be applied to sensorless drives, and the robustness of the strategy can be tested with a parameter sensitivity analysis.

REFERENCES

[1] I. Takahashi and T. Noguchi, "A new quick response and high efficiency control strategy for the induction motor," *IEEE Trans. Ind. Appl.*, vol. IA-22, no. 2, pp. 820–827, Sep./Oct. 1986.

[2] W. Jun, P. Hong, and J. Yu, "A simple direct-torque fuzzy control of permanent magnet synchronous motor drives," in *Proc. 5th WCICA*, Jun. 2004, vol. 5, pp. 4554–4557.

[3] K. M. Tsang and W. L. Chan, "Adaptive control of power factor correction converter using nonlinear system identification," *Proc. Inst. Elect. Eng.—Elect. Power Appl.*, vol. 152, no. 3, pp. 627–633, May 2005.

[4] P. Marino and F. Vasca, "Sliding mode control for three phase rectifiers," in *Proc. 26th Annu. IEEE PESC*, Jun. 1995, vol. 2, pp. 1033–1039.

[5] J. Holtz and S. Stadtfeld, "A predictive controller for the stator current vector of AC machines fed from a switched voltage source," in *Proc. IPEC*, Tokyo, Japan, 1983, pp. 1665–1675.

[6] J. M. Maciejowski, *Predictive Control With Constraints*. Englewood Cliffs, NJ: Prentice-Hall, 2002.

[7] S. Bolognani, S. Bolognani, L. Peretti, and M. Zigliotto, "Design and implementation of model predictive control for electrical motor drives," *IEEE Trans. Ind. Electron.*, vol. 56, no. 6, pp. 1925–1936, Jun. 2009.

[8] S. Mariethoz, A. Domahidi, and M. Morari, "Sensorless explicit model predictive control of permanent magnet synchronous motors," in *Proc. IEEE IEMDC*, May 2009, pp. 1250–1257.

[9] M. P. Kazmierkowski and L. Malesani, "Current control techniques for three-phase voltage-source PWM converters: A survey," *IEEE Trans. Ind. Electron.*, vol. 45, no. 5, pp. 691–703, Oct. 1998.

[10] T. Geyer, G. Papafotiou, and M. Morari, "Model predictive direct torque control—Part 1: Concept, algorithm, and analysis," *IEEE Trans. Ind. Electron.*, vol. 56, no. 6, pp. 1894–1905, Jun. 2009.

[11] G. Papafotiou, J. Kley, K. G. Papadopoulos, P. Bohren, and M. Morari, "Model predictive direct torque control—Part 2: Implementation and experimental evaluation," *IEEE Trans. Ind. Electron.*, vol. 56, no. 6, pp. 1894–1905, Jun. 2009.

[12] P. Cortes, M. P. Kazmierkowski, R. M. Kennel, D. E. Quevado, and J. Rodriguez, "Predictive control in power electronics and drives," *IEEE Trans. Ind. Electron.*, vol. 55, no. 12, pp. 4312–4324, Dec. 2008.

[13] J.-O. Krah and J. Holtz, "High-performance current regulation and efficient PWM implementation for low-inductance servo motors," *IEEE Trans. Ind. Appl.*, vol. 35, no. 5, pp. 1039–1049, Sep./Oct. 1999.

[14] S. Mariethoz and M. Morari, "Explicit model-predictive control of a PWM inverter with an LCL filter," *IEEE Trans. Ind. Electron.*, vol. 56, no. 2, pp. 389–399, Feb. 2009.

[15] M. Pacas and J. Weber, "Predictive direct torque control for the PM-synchronous machine," *IEEE Trans. Ind. Electron.*, vol. 52, no. 5, pp. 1350–1356, Oct. 2005.

[16] J. Beerten, J. Verveckken, and J. Driesen, "Predictive direct torque control for flux and torque ripple reduction," *IEEE Trans. Ind. Appl.*, vol. 57, no. 1, pp. 404–412, Jan. 2010.

[17] C.-Y. Huang, C.-P. Wei, J.-T. Yu, and Y.-J. Hu, "Torque and current control of induction motor drives for inverter switching frequency reduction," *IEEE Trans. Ind. Appl.*, vol. 52, no. 5, pp. 1364–1371, Oct. 2005.

[18] N. Mohan, T. M. Undeland, and W. P. Robbins, *Power Electronics*, 3rd ed. Hoboken, NJ: Wiley, 2003.

[19] S. Dieckerhoff, S. Bernet, and D. Krug, "Power loss-oriented evaluation of high voltage IGBTs and multilevel converters in transformerless traction applications," *IEEE Trans. Power Electron.*, vol. 20, no. 6, pp. 1328–1336, Nov. 2005.

[20] T.-J. Kim, D.-W. Kang, Y.-H. Lee, and D.-S. Hyun, "The analysis of conduction and switching losses in multi-level inverter system," in *Proc. IEEE 32nd Annu. Power Electron. Spec. Conf.*, Jun. 17–21, 2001, vol. 3, pp. 1363–1368.

[21] K. Drobnič, M. Nemec, D. Nedeljkovič, and V. Ambrožič, "Predictive direct control applied to AC drives and active power filter," *IEEE Trans. Ind. Electron.*, vol. 56, no. 6, pp. 1884–1893, Jun. 2009.

[22] S. Kouro, P. Corts, R. Vargas, U. Ammann, and J. Rodrguez, "Model predictive control a simple and powerful method to control power converters," *IEEE Trans. Ind. Electron.*, vol. 56, no. 6, pp. 1826–1838, Jun. 2009.

[23] F. Overney, B. Jeanneret, and A. Mortara, "A synchronous sampling system for high precision AC measurements," in *Proc. CPEM Dig.*, Jun. 2008, pp. 596–597.

Matthias Preindl was born in Brixen, Italy, in 1986. He received the B.Sc. degree (*summa cum laude*) in electrical engineering from the University of Padova, Padova, Italy, in 2008 and the M.Sc. degree in electrical engineering and information technology from the Swiss Federal Institute of Technology (ETH) Zurich, Zurich, Switzerland, in 2010.

He has been a Visiting Student with the Department of Energy Technology, Aalborg University, Aalborg, Denmark, where he wrote his diploma thesis. Aside from the studies, he designed small-sized renewable energy power plants in industry and worked on ITER projects with Ricerca Formazione Innovazione (RFX), Consiglio Nazionale delle Ricerche, Padova. Since 2010, he has been with Leitwind, Sterzing, Italy, where he is an R&D Engineer. His research interests include power electronics and drives and focus on power electronic converters and the modeling and control of electrical machines and turbines.

Erik Schaltz (M'06) was born in Viborg, Denmark, in 1981. He received the M.Sc. and Ph.D. degrees in electrical engineering from the Department of Energy Technology, Aalborg University, Aalborg, Denmark, in 2005 and 2010, respectively.

Since 2009, he has been an Assistant Professor with Aalborg University. His research interests include the analysis, modeling, design, and control of power electronics, electric machines, energy storage devices, fuel cells, and hybrid electric vehicles.

Paul Thøgersen (M'92–SM'01) was born in Thy, Denmark, on June 29, 1959. He received the M.Sc.E.E. degree in control engineering and the Ph.D. degree in power electronics and drives from Aalborg University, Aalborg, Denmark, in 1984 and 1989, respectively.

From 1988 to 1991, he was an Assistant Professor with Aalborg University. Since 1991, he has had a close relationship with Aalborg University, resulting in more than 20 coauthored papers and participation in more than ten Ph.D. student advisory groups. From 1991 to 2005, he was with Danfoss Drives A/S, Grasten, Denmark, where he was first a Research and Development Engineer and later the Manager of Technology, mainly responsible for the drives control technology area. Since 2006, he has been the Manager of the Modeling and Control Group, R&D Department, KK-Electronic A/S, Aalborg.

Dr. Thøgersen was the recipient of the Angelos Award in 1999 for his contributions to the development of industrial drives.